LIQUID CRYSTALS

Programming liquid crystal elastomers for multistep ambidirectional deformability

Yuxing Yao[1,2]†, Atalaya Milan Wilborn[3]†, Baptiste Lemaire[3], Foteini Trigka[4], Friedrich Stricker[3], Alan H. Weible[5], Shucong Li[1], Robert K. A. Bennett[3]‡, Tung Chun Cheung[3], Alison Grinthal[3], Mikhail Zhernenkov[6], Guillaume Freychet[6], Patryk Wąsik[6], Boris Kozinsky[3,7], Michael M. Lerch[3,4]*, Xiaoguang Wang[3,5]*, Joanna Aizenberg[1,3]*

Ambidirectionality, which is the ability of structural elements to move beyond a reference state in two opposite directions, is common in nature. However, conventional soft materials are typically limited to a single, unidirectional deformation unless complex hybrid constructs are used. We exploited the combination of mesogen self-assembly, polymer chain elasticity, and polymerization-induced stress to design liquid crystalline elastomers that exhibit two mesophases: chevron smectic C (cSmC) and smectic A (SmA). Inducing the cSmC-SmA–isotropic phase transition led to an unusual inversion of the strain field in the microstructure, resulting in opposite deformation modes (e.g., consecutive shrinkage or expansion and right-handed or left-handed twisting and tilting in opposite directions) and high-frequency nonmonotonic oscillations. This ambidirectional movement is scalable and can be used to generate Gaussian transformations at the macroscale.

Small-molecule liquid crystals (LCs) are a class of compounds capable of self-aligning and forming various self-assembling organized mesophases, giving rise to anisotropic material properties (*1*, *2*). For example, rod-shaped mesogens, comprising a rigid aromatic core and a short aliphatic tail, generally organize into a nematic (N) phase characterized by long-range orientational order but lacking positional order. Lengthening the aliphatic tail strengthens intermesogenic interactions, leading to the formation of a smectic A (SmA) phase characterized by both long-range orientational and short-range positional order, with mesogens arranged in parallel lamellae. The specific configurations accessed by these small-molecule mesogenic compounds depend on molecular shape, microsegregation, and topology (*3*). Variations in these parameters intricately dictate the geometric packing arrangements and the phase diagram of the resulting assemblies, enabling broad applications including displays (*4*), controlled drug delivery (*5*), and biosensors (*6*).

Liquid crystalline elastomers (LCEs) are soft materials that combine the self-assembly of LCs with the rubbery elasticity of a lightly cross-linked polymer network in a single material (*7*–*9*). Transitioning from aligned LC packing to a disordered isotropic (Iso) state translates mesogenic motion into directional reconfiguration of the polymer chains, resulting in a macroscopic deformation. Therefore, LCEs have been explored as soft robotic actuators capable of performing various tasks such as swimming (*10*), gripping (*11*), and artificial muscle actuation (*12*), and exhibiting unique properties such as auxetic (*13*) and photonic (*14*) behavior. Leveraging LC phase change as the driving force for deformations allows for versatile actuations under stimuli such as heat (*15*), light (*16*, *17*), and humidity (*18*), thus expanding their applicability. In contrast to small-molecule LCs, in which LC packing relies solely on intermesogenic interactions, the arrangement of LCs in LCEs is typically constrained by mesogen-polymer coupling and interpolymer chain interactions (*8*), which limit the presence of multiple LCE mesophases and subsequent chain reconfigurations to a single transition. For example, when mesogens are covalently attached to polymer chains in main-chain or side-chain side-on (referred to as "side-on") configurations, the two most common LCE structures studied and used so far, their collinearity with polymer chains restricts their rotational freedom and ability to rearrange (Fig. 1A, top). As a result, these LCEs predominantly exhibit only one mesophase and one corresponding mesophase-Iso phase transition observed as a one-step uniaxial strain, most commonly leading to material contraction along the alignment axis of mesogens, referred to as the LC director (Fig. 1B, top) (*19*). Designing a structure capable of multiple deformations in response to a single stimulus requires hybrid material constructs (*20*, *21*), as well as complex and precise architectures (*22*–*24*) and/or a stimulus field (*10*, *12*, *25*), which entails sophisticated implementation (*26*–*28*) and exhibits strong length-scale dependence (*20*, *22*–*25*). We posit that strategic chemical design can overcome these limitations by establishing a delicate synergy among intermesogenic interactions, mesogen-polymer coupling, and polymer network constraints, giving rise to a rich phase behavior and multistep deformability and opening doors to multimodal, single-material actuators.

We introduce three design principles: (i) aligning the LC monomers before polymerization, (ii) creating a less rotationally constrained side-chain end-on mesogen-polymer attachment (referred to as "end-on"; Fig. 1A, bottom), and (iii) taking advantage of the directional stress build-up upon polymerization of prealigned mesogens. These principles were used to create a class of end-on LCEs (Fig. 1C) that exhibit two high-order mesophases, namely chevron smectic C (cSmC) and SmA, even though only the N phase is formed in their aligned LC monomers. The emergence of these phases was predicted by molecular dynamics (MD) simulations and comprehensively analyzed by wide-angle/small-angle x-ray scattering (WAXS/SAXS), differential scanning calorimetry (DSC), and polarized light microscopy. We observed cSmC-SmA-Iso phase transitions that enable a multistep actuation behavior with ambidirectionality, such as contraction followed by expansion, consecutive right- and left-handed twisting, or switching of the tilt direction relative to the room temperature reference state (Fig. 1B, bottom). Such ambidirectional deformations were not observed in single-transition LCEs (Fig. 1B, top) or in a small number of previously reported multiphase LCEs involving SmA-N-Iso or chiral SmC-SmA-Iso transitions, which displayed either monotonic deformations or an inability to deform beyond the reference state (fig. S1) (*29*, *30*).

Effects of mesogen-polymer interactions on phase behavior of end-on LC polymers

We anticipated that a family of end-on LCEs derived from the polymerization of prealigned LC monomers with a terminal acrylate group (Fig. 1C) may offer multiple phase transitions because of the presence of (i) the flexible linker of appropriate length (l), which will provide sufficient rotational freedom to the mesogen within a loosely cross-linked polymer network; (ii) the alkyl tail of appropriate length (m) that will promote mesogenic self-assembly; and (iii) the shrinkage stress that has been reported to develop upon polymerization of acrylates (*31*).

To investigate the potential impact of such a structure on the LCE phase behavior, we first performed MD simulations of a representative member of this family with $l = 6$ and $m = 5$ – [4-(6-acryloxy-hex-1-yl-oxy)phenyl 4-(hexyloxy)benzoate] (Fig. 1D and supplementary text, section 1). Mesogen representation in MD simulations is shown in fig. S2. By equilibrating the simulated

[1]Department of Chemistry and Chemical Biology, Harvard University, Cambridge, MA, USA. [2]Department of Chemical and Biological Engineering, The Hong Kong University of Science and Technology, Clear Water Bay, Kowloon, Hong Kong, China. [3]Harvard John A. Paulson School of Engineering and Applied Sciences, Harvard University, Cambridge, MA, USA. [4]Stratingh Institute for Chemistry, University of Groningen, Groningen, Netherlands. [5]Department of Chemical and Biomolecular Engineering, The Ohio State University, Columbus, OH, USA. [6]National Synchrotron Light Source II, Brookhaven National Laboratory, Upton, NY, USA. [7]Bosch Research, Watertown, MA, USA.
***Corresponding author. Email: m.m.lerch@rug.nl (M.M.L.); wang.12206@osu.edu (X.W.); jaiz@seas.harvard.edu (J.A.)**
†These authors contributed equally to this work.
‡Present address: Department of Electrical Engineering, Stanford University, Stanford, CA, USA.

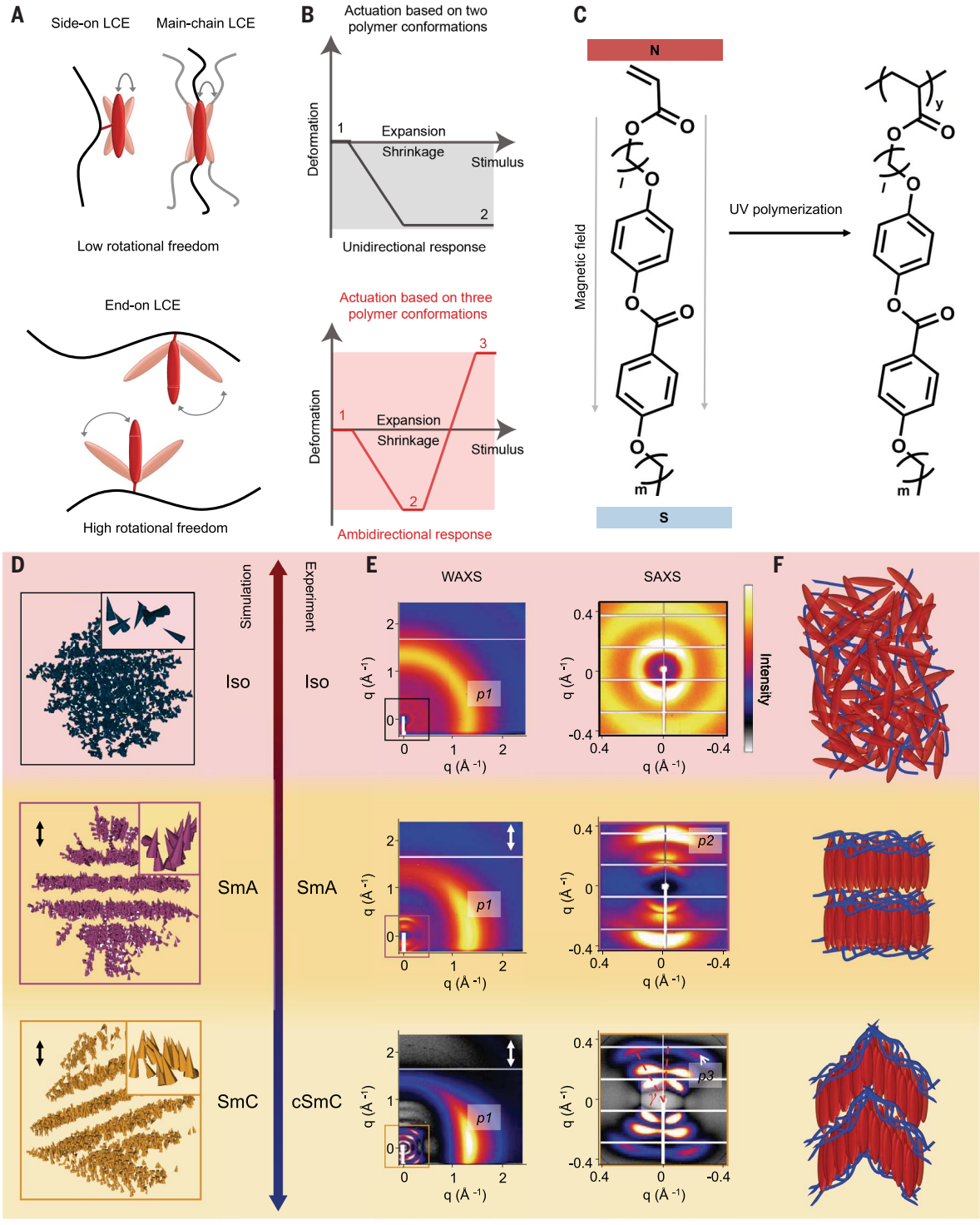

Fig. 1. Multiphase behavior of end-on LCEs. (**A** and **B**) Schematics showing the enhanced rotational freedom (A) and differences in encoded deformability (B) displayed by end-on LCEs (bottom) compared with their side-on and main-chain counterparts (top). (**C**) Photopolymerization of proposed family of end-on mesogenic monomers prealigned in a magnetic field. (**D**) MD simulation box with 1000 mesogens showing Iso (top), SmA (middle), and monodomain SmC (bottom) phases upon simulated polymerization of an end-on LC monomer [4-(6-acryloxy-hex-1-yl-oxy)phenyl 4-(hexyloxy)benzoate]. Each arrow-cone represents a mesogen, with the base located at the reactive acrylate site and pointing toward the alkyl tail, to show relative directionality of each mesogen. Mesogens in the SmA and monodomain SmC phases align along a spontaneous director vector (shown as a black double arrow) through equilibration in MD simulations. (**E**) 2D WAXS (left) and SAXS (right) of the above LCE at 150°C (top; Iso), 100°C (middle; SmA), and 25°C [bottom; chevron SmC (cSmC)]. The x-ray beam was irradiated perpendicular to the mesogenic director of the sample. γ defines the angle between the normal to the lamellae and the director axis in cSmC phase. (**F**) Schematic representation of molecular packing in the Iso (top), SmA (middle), and cSmC (bottom) phases, with mesogens and polymer chains depicted as red ovals and blue threads, respectively. Double-headed arrows in (D) and (E) indicate the mesogenic director.

unpolymerized system stepwise from 180° to 50°C, we observed one phase transition from the Iso to the N phase in which monomeric mesogens spontaneously aligned along the LC director (fig. S3). We subsequently modeled the polymerization of nematically oriented monomers by connecting neighboring acrylate groups and observed the formation of two lamellar mesophases, SmA and monodomain smectic C (SmC), which were not present in the respective end-on LC monomers (Fig. 1D and fig. S4, A to D). Crucially, MD simulations predict distinct polymer chain conformations for each of the three mesophases, namely random coil in the Iso phase, two-dimensional (2D) confinement between neighboring lamellae in the SmA phase, and similar 2D confinement between tilted lamellae in the SmC phase (fig. S4E).

To experimentally validate the phase behavior of the end-on LC system, we used WAXS/SAXS measurements (see the supplementary text, section 2) to monitor the real-time evolution of mesogenic packing of [4-(6-acryloxy-hex-1-yl-oxy)phenyl 4-(hexyloxy)benzoate] monomers placed in a magnetic field to encode uniaxial *Z*-axis alignment. At 100°C, end-on LC monomers are in the Iso phase, exhibiting a diffusive ring that narrows when cooled to 40°C, suggesting a uniaxial alignment of monomers in N phase and in agreement with the simulation results (fig. S5, A and B). Detailed WAXS/SAXS analysis of the polymerized end-on LCE cross-linked with 1,6-hexanediol diacrylate (HDDA, 5% wt/wt relative to monomer mass), a nonmesogenic cross-linker, revealed the following: (i) at 150°C, the elastomer is in Iso phase (Fig. 1E, top), with an azimuthally diffusive ring at $d_{intermesogen}$ = 4.75Å (designated as ***p1*** in the WAXS); (ii) cooling to 100°C, ring ***p1*** narrowed, and another set of peaks, ***p2***, appeared perpendicular to peak ***p1*** in the SAXS region, which is characteristic of a *Z*-aligned SmA phase (Fig. 1D, middle) (*32*) with the lamellar spacing d_{SmA} = 18.2Å; (iii) upon further cooling to 30°C, a chevron SmC (cSmC) phase appeared with the mesogens remaining aligned along the *Z*-axis but with an angle to the formed lamellae, as evidenced by the peak ***p1*** profile similar to that of SmA phase and the splitting of the peaks, ***p3***, in the SAXS region (*33*) (Fig. 1E, bottom). The layer thickness d_{cSmC} was measured to be 16.5 Å, with a chevron-tilting angle $\gamma = 35°$. In all three phases, the mesogenic packing was random in the plane perpendicular to the director (fig. S6). The phase behavior described above was also confirmed by polarized light microscopy imaging (fig. S7). The observed cSmC-SmA-Iso phases depicted in Fig. 1F remained generally the same for end-on LC polymers obtained with (Fig. 1E) and without (figs. S5C and S8) the HDDA cross-linker, suggesting that these transitions are intrinsically encoded in the chemical structure of end-on LCEs. DSC analysis (fig. S9) confirmed one phase transition in the monomeric state and two phase transitions for the elastomers.

Effects of intermesogenic interactions and polymer network constraints on phase behavior of end-on LC polymers

Past studies in both monomeric LCs and polymerized LCEs have demonstrated that the molecular structure of mesogens, e.g., the aliphatic tail, influences intermesogenic interactions, consequently steering the packing into various phases (*34*). To investigate how intermesogenic interactions affect the end-on LCE phase behavior illustrated in Fig. 1E while keeping the degree of mesogen-polymer coupling largely unaffected, we synthesized a series of end-on LC monomers with the same linker length (l = 6) but different tail lengths (fig. S10). The appearance of the cSmC and SmA phases is typical for this series, albeit at different transition temperatures (table S1). The only exception was observed for the shortest tail length (m = 0), where LCEs only display N phase due to insufficient intermesogenic interactions for lamellar formation (Fig. 2, A and B, and fig. S11). To assess the effect of mesogen-polymer coupling, we synthesized an end-on LC mesogen with a short linker connection to the polymer chain (l = 2) (fig. S10). Not unexpectedly, this modification reduced rotational freedom of mesogens relative to the polymer, inhibiting the formation of any ordered mesophases (Fig. 2B and fig. S12). We further investigated the influence of polymer network constraints on LCE phase behavior by increasing the cross-linking density, which produced a more conformationally restrictive network, reducing mesogenic freedom and thus the number of achievable phases within the system (Fig. 2C). As confirmed by DSC and polarized light microscopy imaging (figs. S7 and S13), although two mesophases were observed with HDDA concentration <15%, an increase to 17.5% constrained the mesogens, preventing the formation of the cSmC phase and resulting in only the SmA phase. Further increase to 20% prevented the assembly of mesogens into any ordered mesophase (Fig. 2D and fig. S13). Moreover, tuning the length of the nonmesogenic cross-linker (Fig. 2C) provides another way to control chevron packing through polymer network constraints, in which longer cross-linkers induce a lower chevron tilt angle γ (Fig. 2E and fig. S14). This end-on LCE system also allows for the incorporation of functional molecules such as azobenzene-derived cross-linkers while maintaining cSmC-SmA-Iso phase behavior with the first phase transition temperature as low as 55°C (fig. S15).

Ambidirectional mechanical deformations in end-on LCEs

To test the bulk mechanical responses originating from the molecular reconfigurations upon cSmC-SmA-Iso phase transitions, we fabricated LCE microplates with a programmed arbitrary director alignment by placing monomer-filled molds in the desired orientation in magnetic fields and then polymerizing the oriented samples (fig. S16) (*35*–*37*). The two consecutive phase transitions with their characteristic polymer chain conformations (Fig. 1F and fig. S4E) gave rise to distinctive nonmonotonic, ambidirectional fundamental deformation modes (Fig. 3A and movie S1). In particular, upon heating from room temperature to 100°C, microstructures with *Z*-aligned mesogens shrank by 8% along the director axis, and when heated further to 150°C expanded by 20% along the same axis beyond the reference cSmC state (or 12% expansion relative to the reference state; Fig. 3B). In addition to uniaxial contraction or elongation, we demonstrated other types of ambidirectional deformations by magnetically aligning the LCEs off the principal axes of the microplates. The uniaxial shrinkage and biaxial expansion through the cSmC-SmA phase transition created shear in a plane parallel to the director. When this plane aligned with the side walls of the microplate, we observed both out-of-plane (director parallel to the *X*-*Z* plane; Fig. 3C) and in-plane (director parallel to the *Y*-*Z* plane; Fig. 3D) tilting, with structures sequentially tilting by ~12° to the left (or downward) and then by ~20° to the right (or upward) upon heating (movie S1). Conversely, when the shear occured on the top surface of the microplate, the strong adhesion of the bottom surface to the substrate prevented it from shearing, resulting in consecutive right- and left-handed twisting (director oriented 45° from both axes in the *X*-*Y* plane; Fig. 3E) upon heating (movie S1) (*35*). Such two-step opposite deformations were reversible for at least 2000 cycles (fig. S17). The experimentally observed deformations were further confirmed using finite element simulations (Fig. 3F; fig. S18; and supplementary text, section 3) (*38*). The strain magnitude could be adjusted by varying the cross-linker concentration. For instance, 1% wt/wt HDDA resulted in a 32% expansion during the SmA-Iso transition (or 25% expansion relative to the reference state) (fig. S19).

Tunable tonicity and frequency of end-on LCE shape changes

We sought to unlock multiple tones of response (sets of sequential deformations) by varying the operational temperature ranges (Fig. 4, A to C). Taking LCE microplates that exhibit out-of-plane tilting as an example (Fig. 3C), the relationship between tilting angle versus temperature can be easily switched from a monotonic decrease (i.e., the tilting angle decreases with increase in temperature from 70° to 110°C) equivalent to tilting left, to a monotonic increase (i.e., the tilting angle increases with increase in temperature from 110° to 150°C) equivalent to

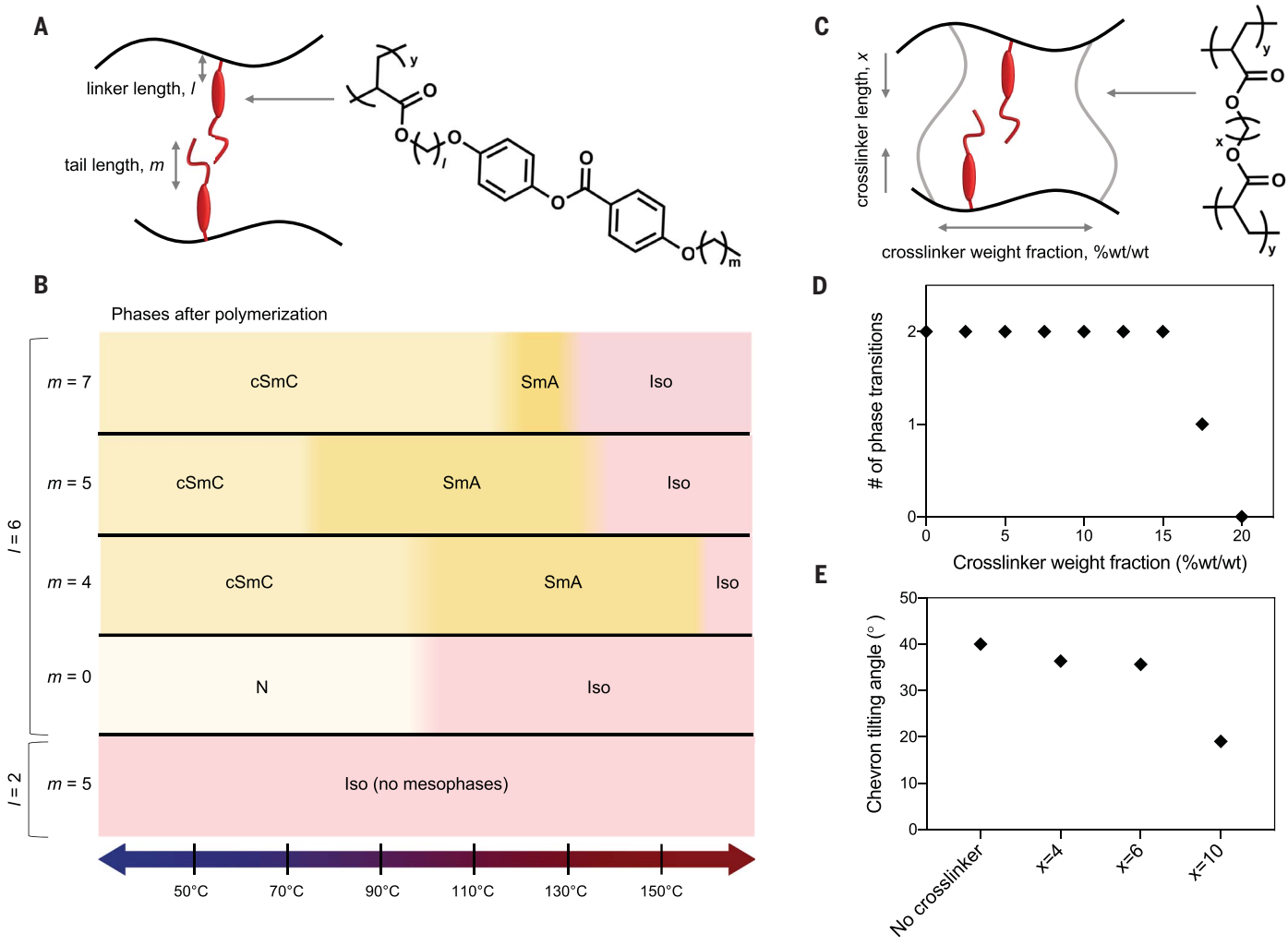

Fig. 2. Effect of mesogenic and polymeric structures on end-on LCE phase behavior. (**A** and **B**) Schematic (A) and experimental (B) results demonstrating the impact of the tail (*m*) and linker (*l*) lengths of end-on LC monomers on the phase behavior of end-on LCEs. (**C**) Schematic indicating the impact of cross-linker length (*x*) on the mesogenic packing in end-on LCEs (left) and molecular structure of the nonmesogenic cross-linkers used in this work (right). (**D**) Number of end-on LCE phase transitions as a function of cross-linker (HDDA, *x* = 6) weight fraction relative to the mass of end-on LC monomer. (**E**) cSmC tilting angle (γ) as a function of cross-linker length with a cross-linker weight fraction of 5% wt/wt relative to the mass of monomers.

tilting right, and a nonmonotonic function (i.e., the tilting angle first decreases and then increases upon heating from 70° to 150°C) equivalent to tilting left and then right from the reference upright position (Fig. 4, A to C, dashed lines, and movie S2).

The demonstrated contact heating–based ambidirectional actuation can be further optimized to achieve remote high-frequency actuation as needed in soft robotic applications. By coating carbon nanotubes onto end-on LCE microstructures and controlling the intensity and frequency of a pulsed infrared laser, we can accurately tune the internal equilibrium temperature of the system through photothermal heating (fig. S20), and thus guide the tilt direction of oscillating microstructures by light (Fig. 4, A to C, solid pale lines). The actuation frequency increases from ~0.01 Hz (through contact heating) to ~1 Hz (with infrared laser), and any desired sequence of oscillations can be programed by changing the intensity and frequency of IR irradiation (Fig. 4D).

Phase-dependent Gaussian curvature of macroscale end-on LCE disks

We anticipated that the ability of these three-phase end-on LCEs to change direction of the strain field during sequential phase transitions could be readily transferred to a large-scale compositionally homogeneous artificial system and combined with programmed LCE alignment to enable complex mechanical actuations macroscopically, such as Gaussian curvature (*K*) reversal.

In-plane radial strain fields have been widely studied as a mechanism for inducing out-of-plane deformations (*24*, *28*, *39*, *40*). For example, flat disks ($K = 0$) were shown to buckle into either saddle ($K < 0$) or dome ($K > 0$) shapes, depending on the direction of the strain field. We used magnetic fields to develop a robust strategy for encoding a radial director field in large end-on LCE sheets (Fig. 5A). Finite element analysis predicted that radial contraction and corresponding circumferential expansion due to Poisson effects generate negative Gaussian curvature in LCE disks when going through a cSmC-SmA transition, whereas a radial expansion and circumferential contraction drive positive Gaussian curvature during a SmA-Iso phase transition (Fig. 5, B and C). This simulation was validated by experimental observations showing how the same end-on LCE disk can transform sequentially to a saddle and then further to a dome (Fig. 5D; fig. S21; movie S3; and supplementary text, section 4). By equilibrating at different temperatures and repeating multiple heating and cooling cycles, we confirmed that these shapes are thermodynamically stable states governed by temperature, rather

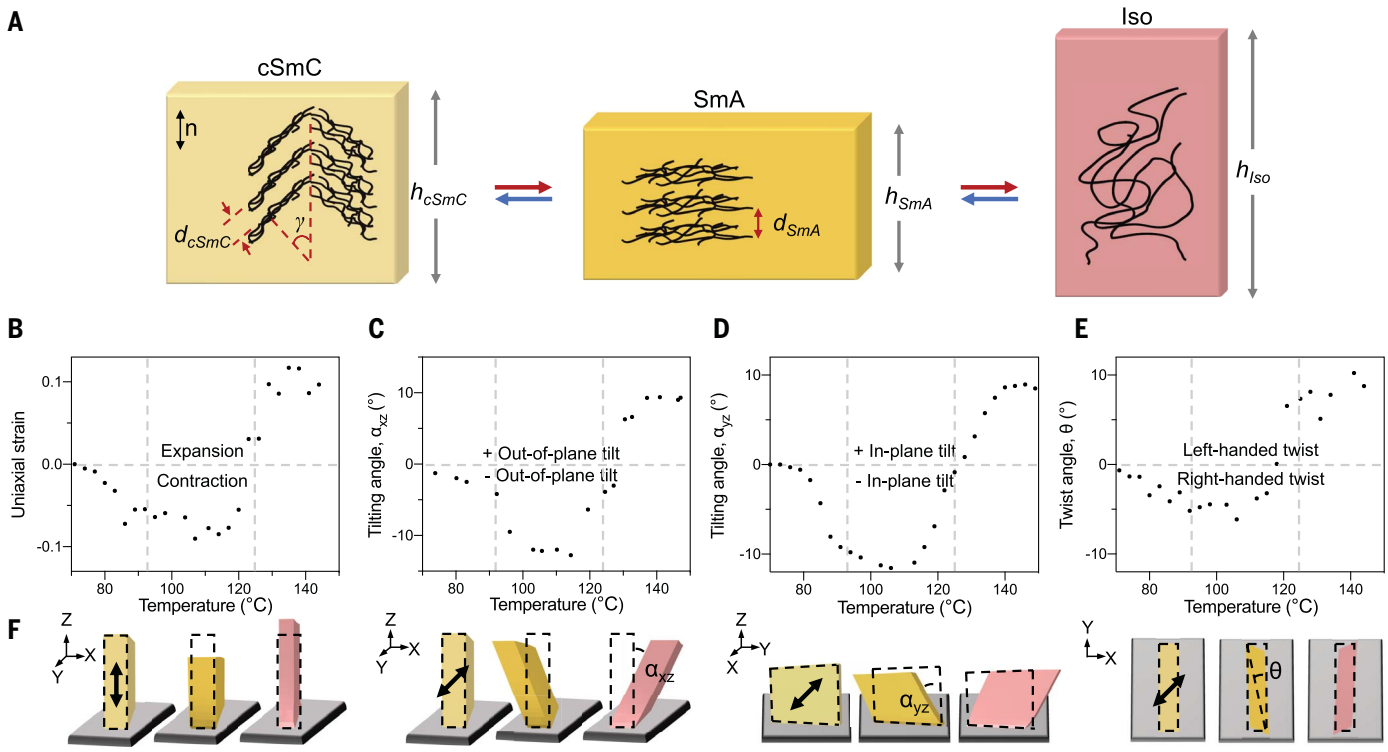

Fig. 3. Temperature-responsive ambidirectional deformations of end-on LCEs. (**A**) Schematic illustrating polymer chain reconfiguration during cSmC-SmA-Iso phase transitions enabling consecutive opposite deformations in end-on LCEs. The schematic blocks illustrate the dimensions of end-on LCE microplates. *h* and *d* denote the height of LCE microplate and lamellar layer thickness, respectively. Black lines inside schematic blocks denote polymer backbones. (**B** to **E**) Experimental observations of various temperature-responsive, ambidirectional modes of deformation in LCE microplates (250 × 50 × 200 μm): uniaxial shrinkage and expansion (B), out-of-plane tilting (C), in-plane tilting (D), and twisting (E). (**F**) Corresponding finite element simulation. Light yellow, dark yellow, and red blocks represent the cSmC, SmA, and Iso phases of LCEs, respectively. Black double-headed arrows in (F) represent the mesogenic alignment within LCE microstructures as determined by the magnetic field applied to molded monomer mixtures. The results in this figure and in Figs. 4 and 5 correspond to the following formulation: End-on monomer (m = 5, l = 6) with 5% wt/wt HDDA and 2% wt/wt photoinitiator.

than being induced by inhomogeneous strains from defects or residual stresses (fig. S21 and movie S4).

In addition to thermal stimuli, we also showed that ambidirectional Gaussian shape morphing can be achieved through solvent-induced swelling, as illustrated by the radially aligned, flat LCE film gradually deforming into saddle and dome shapes with an increasing concentration of acetone in water (fig. S22).

Discussion

In this work, we have demonstrated that rationally designing molecular modifications that synergize polymerization stress and intermesogenic, mesogen-polymer, and polymer-polymer interactions within end-on LCEs provides a platform with which to create a class of elastomers with rich phase behaviors (and thus, deformations) that have not yet been observed in main-chain and side-on LCEs and their respective unpolymerized small-molecule LC monomers. In particular, by both extensive MD simulations and x-ray diffraction studies, we have shown the emergence of lamellar SmA and cSmC mesophases that form only upon polymerization of end-on LC mesogens and do not appear in a nematically organized monomeric state.

We reason that the mechanism for the assembly into high-order smectic mesophases (cSmC in particular) is a combination of (i) mesogen alignment predetermined before polymerization, (ii) end-on mesogen-polymer attachment configuration for rotational freedom of mesogens, and (iii) shrinkage stress buildup upon polymerization of nematically aligned acrylate monomers that leads to the formation of lamellar structures facilitated by the aliphatic tail interactions and their further transition to a chevron configuration with sufficient stress (fig. S23 and supplementary text, section 5). Transformation of a uniaxially aligned system to a biaxial, chevron geometry commonly occurs to accommodate stresses under applied strain. Indeed, shrinkage stress on the order of megapascals has been reported to develop upon polymerization of acrylates (*31*), and similar stress values were sufficient to generate chevron structures upon uniaxial stretching of LCEs (*33*, *41*). To substantiate this mechanism, we performed the polymerization in the presence of a stress-releasing agent and observed only SmA lamellae formation, but no cSmC phase, in the resulting LCE (fig. S24). The same mechanism is further supported by the results shown in Fig. 2, D and E, where cSmC tilting angle γ decreases with longer cross-linkers, which are likely to reduce the pulling force to rotate the lamellae. The lamellar mesophases, which are crucial to the observed multistep deformation behavior, can be readily modulated through the rational design of molecular architecture. We foresee that harnessing directional polymerization stress and molecular engineering can provide a general strategy to achieve higher-order packings in other (meso)phases, thereby extending structure-related functionalities in soft matter.

The cSmC-SmA-Iso transitions give rise to nonmonotonic, ambidirectional deformations, which can be explained by the following considerations (see the supplementary text, section 6). During the cSmC-SmA phase transition, the tilted lamellae flatten, maintaining the direction of mesogenic director while compressing polymer chains and driving macroscopic contraction along $\bar{n}$ ($h_{cSmC} > h_{SmA}$). Indeed, the observed 8% shrinkage (Fig. 3B) is in agreement with the calculated theoretical strain of

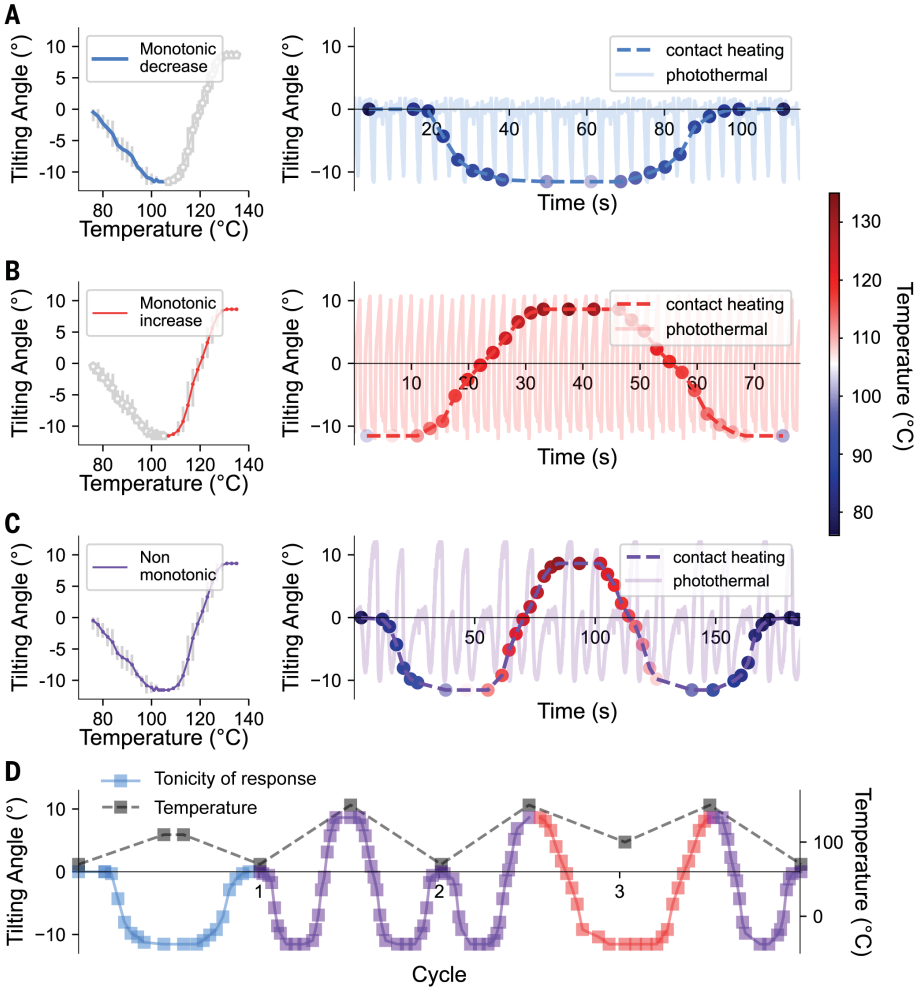

Fig. 4. Stimuli-responsive tonicity and frequency of end-on LCE oscillations. (**A** to **C**) Tunable tonicity of mechanical responses of the same end-on LCE microstructure through selection of a temperature range (illustrated by the colored solid lines on the left panel): monotonically decreasing (A), monotonically increasing (B), and nonmonotonic shape deformation (C). Dashed bright lines show results for contact heating, and pale solid lines represent oscillations by infrared laser through the photothermal effect. Dots in different colors mark the temperature of end-on LCEs. Error bars (gray) mark the SD of three independent experiments. (**D**) Programmed variations in temperature (dashed gray lines) define the tonicity of the mechanical response of the same end-on LCE microplate (solid lines). Blue, red, and purple curves illustrate monotonically decreasing, monotonically increasing, and nonmonotonic mechanical responses, respectively.

~10% imposed by the lamellar rotation during the cSmC-SmA transition. Transitioning further from the SmA to the Iso phase, polymer chains relax into the entropically favorable random coil configuration, in which they occupy space in all directions with equal probability, leading to a macroscopic 20% expansion along $\bar{n}$ ($h_{Iso} > h_{SmA}$). In contrast to the traditional monotonic decrease in mesogenic order with increasing temperature (i.e., the scalar order parameter S_{LC} calculated from the peak intensities in the x-ray patterns decreases from 0.61 in the cSmC phase, to 0.39 in the SmA phase, and to 0.05 in the Iso phase), the estimated conformational entropy of polymer chains exhibits an unconventional temperature dependence: Temperature increase results in an initial 2.3% decrease in order, followed by a 3.7% increase. We hypothesize that this nonmonotonic change in polymer chain order is compensated by the constant entropy gain introduced by mesogen rearrangement, highlighting the importance of interplay between mesogenic packing and polymer network elasticity in obtaining rich phase and deformation behaviors.

Unlike previous strategies to realize complex deformations in soft matter by introducing chemical and/or mechanical heterogeneity within materials, including inhomogeneous or externally programmed stimuli fields (*10*, *25*, *28*, *40*) or multicomponent structural composites (*22*, *42*), the ability of end-on LCEs to switch the sign of the strain field during the sequential phase transitions made it possible to achieve multi-step ambidirectional deformations in chemically homogeneous micro- and macroscopic LCE-based soft actuators using a simple, scalable fabrication procedure. By taking advantage of magnetic fields to encode a desired mesogenic orientation before polymerization (*35*–*37*), we readily and reliably achieved a variety of basic, fully reversible nonmonotonic deformations of nascent LCE architectures, such as sequential contraction-expansion, ambidirectional tilting, and right- and left-handed twisting, in response to monotonic temperature increase. Furthermore, this system is also tunable to enable distinct oscillatory ambidirectional movements under different temperature ranges, including high-frequency oscillations in response to light using photothermal heating. Any desired sequence of monotonic or nonmonotonic microstructure oscillations can be programmed by "reading" a prescribed temperature sequence controlled by the intensity of a laser light, enabling remote control of microstructure movements. The achieved oscillation frequency of ~1 Hz is comparable to the actuation frequency of human cardiomyocytes (*43*), suggesting that these mechanical actuations with switchable tonicity and frequency may find applications in mimicking the biological mechanical actuations in artificial soft robotics (*44*). Our demonstration of centimeter-scale LCE disks that sequentially switch Gaussian curvature and undergo a disk-saddle-dome transition upon temperature increase provides convincing evidence that the ambidirectionality of deformations can be extended to macroscale objects across three orders in dimensions. Gaussian curvature is a fundamental geometric factor that plays a critical role in motion in nature, such as in nastic motion in plants (*45*), membrane fission in cells (*46*), and motility in marine life (*47*). The ability to encode a desired gradient in the radial director orientation in large end-on LCE sheets using magnetic alignment offers an opportunity to fine-tune the in-plane strain field, leading to dynamic actuations of single-material structures undergoing multiple shape reconfigurations across the entire spectrum of Gaussian curvature that were previously difficult to achieve.

Beyond thermal stimuli, we have demonstrated that ambidirectional deformations can also be achieved through solvent-induced swelling, further highlighting the key role of the strain field in LCE molecular reconfigurations. Moreover, incorporating photoresponsive cross-linkers can extend these behaviors to enable photoactuation. Our class of three-phase end-on LCEs demonstrates an array of new emergent properties, opening avenues in numerous soft robotic applications from ambidirectional actuators to swimmers. These LCEs can lift weight 450 times greater than their own, showcasing their potential as an artificial muscle (fig. S25 and movie S5). They may further enable other complex

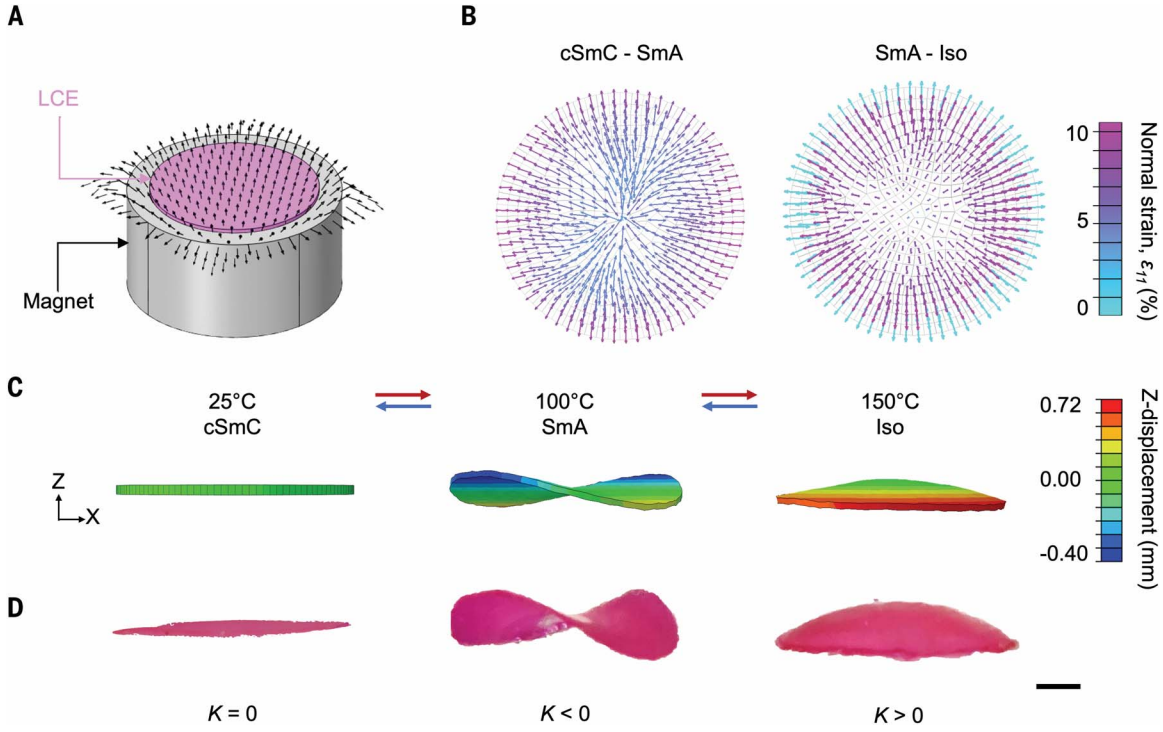

Fig. 5. Macroscale LCE disk with Gaussian curvature reversion. (**A**) Schematics illustrating the spatial patterning of mesogenic director encoded in a macroscale end-on LCE disk with a magnetic field. (**B**) Calculated normal strain in the radial direction for an end-on LCE disk upon the cSmC-SmA (left) and the SmA-Iso (right) phase transition. Radial strain is higher along the edges compared with the center during the cSmC-SmA transition and then switches to its lowest along the edges during SmA-Iso transition, indicating a directional change in strain between the two transitions. (**C** and **D**) Finite element simulations (C) and experimental results (D) demonstrating the transformation of the initially flat end-on LCE disk (1 cm in diameter × 230 μm thick) into a saddle shape with negative Gaussian curvature and further into a dome shape with positive Gaussian curvature as temperature increases. Pink coloration of LCE films in (D) is caused by doping with rhodamine B for better visualization. Scale bar, 2 mm.

functions, such as self-regulatory behaviors generally used by biological systems to maintain mechanical and chemical homeostasis and function in changing environments. For example, stomatal cells balance hydration levels through water exchange. Their openings increase with temperature up to 35°C and then decrease to prevent excessive dehydration (fig. S26A) (*44*). Our end-on LCEs, with their ambidirectional response to temperature through sequential contraction and expansion upon phase change, are ideal for designing artificial stomatal cells: Slits cut into end-on LCE films are able to mimic this homeostatic behavior (fig. S26, B to D, and movie S6). Compared with previous methods requiring complex temperature control systems or the introduction of mechanical heterogeneity, our approach achieves similar functions with only one material that can directly interface with the environmental changes. This enhances the practicality and functionality of LCEs and substantially simplifies potential configurations in soft robotics.

The family of end-on LCEs described here represents just one example within a wide range of LCEs in which the synergy among mesogen-polymer, mesogen-mesogen, and polymer-polymer interactions facilitated by a directional polymerization stress plays an important role in introducing complex phase behaviors. Our molecular-centered strategy is complementary to existing ones, including dynamic covalent bonds (*21*), the synergistic use of photochemical and photothermal effects (*48*), manually assembled director patterns (*26*), and selective polymer chain de-cross-linking (*27*), to enable more complex deformability.

REFERENCES AND NOTES

1. M. Kleman, O. D. Lavrentovich, *Soft Matter Physics: An Introduction* (Springer, 2003).
2. R. Zhang, A. Mozaffari, J. J. de Pablo, *Nat. Rev. Mater.* **6**, 437–453 (2021).
3. C. P. Lapointe, T. G. Mason, I. I. Smalyukh, *Science* **326**, 1083–1086 (2009).
4. I. Muševič, *Liq. Cryst. Rev.* **4**, 1–34 (2016).
5. Y.-K. Kim, X. Wang, P. Mondkar, E. Bukusoglu, N. L. Abbott, *Nature* **557**, 539–544 (2018).
6. I.-H. Lin *et al.*, *Science* **332**, 1297–1300 (2011).
7. T. J. White, D. J. Broer, *Nat. Mater.* **14**, 1087–1098 (2015).
8. C. Ohm, M. Brehmer, R. Zentel, *Adv. Mater.* **22**, 3366–3387 (2010).
9. A. Gruzdenko, I. Dierking, *Front. Soft Matter* **2**, 1052037 (2022).
10. S. Palagi *et al.*, *Nat. Mater.* **15**, 647–653 (2016).
11. O. M. Wani, H. Zeng, A. Priimagi, *Nat. Commun.* **8**, 15546 (2017).
12. S. Li *et al.*, *Sci. Adv.* **7**, eabg3677 (2021).
13. D. Mistry *et al.*, *Nat. Commun.* **9**, 5095 (2018).
14. S.-U. Kim *et al.*, *Nat. Mater.* **21**, 41–46 (2022).
15. G. Chen *et al.*, *Nat. Commun.* **14**, 6822 (2023).
16. J. A. Lv *et al.*, *Nature* **537**, 179–184 (2016).
17. A. Ryabchun *et al.*, *Chem* **9**, 3544–3554 (2023).
18. L. T. de Haan, J. M. Verjans, D. J. Broer, C. W. Bastiaansen, A. P. Schenning, *J. Am. Chem. Soc.* **136**, 10585–10588 (2014).
19. T. H. Ware, M. E. McConney, J. J. Wie, V. P. Tondiglia, T. J. White, *Science* **347**, 982–984 (2015).
20. M. Zhang, A. Pal, X. Lyu, Y. Wu, M. Sitti, *Nat. Mater.* **23**, 560–569 (2024).
21. Y. Wu *et al.*, *Sci. Adv.* **8**, eabo6021 (2022).
22. Y.-Y. Xiao, Z.-C. Jiang, J.-B. Hou, Y. Zhao, *Nat. Commun.* **12**, 624 (2021).
23. M. Wang, B.-P. Lin, H. Yang, *Nat. Commun.* **7**, 13981 (2016).
24. S.-J. Jeon, A. W. Hauser, R. C. Hayward, *Acc. Chem. Res.* **50**, 161–169 (2017).
25. T. Zhao *et al.*, *J. Mater. Chem. C* **10**, 3796–3803 (2022).
26. X. Zeng *et al.*, *Crystals* **14**, 357 (2024).
27. Z. C. Jiang, Y. Y. Xiao, X. Tong, Y. Zhao, *Angew. Chem. Int. Ed.* **58**, 5332–5337 (2019).
28. B. A. Kowalski, C. Mostajeran, N. P. Godman, M. Warner, T. J. White, *Phys. Rev. E* **97**, 012504 (2018).
29. N. Aßfalg, H. Finkelmann, *Macromol. Chem. Phys.* **202**, 794–800 (2001).
30. K. Hiraoka, N. Tagawa, K. Baba, *Macromol. Chem. Phys.* **209**, 298–307 (2008).
31. A. A. Stolov, T. Xie, J. Penelle, S. L. Hsu, *Macromolecules* **33**, 6970–6976 (2000).
32. W. H. de Jeu, A. Komp, E. P. Obraztsov, B. I. Ostrovskii, H. Finkelmann, *Soft Matter* **5**, 4922–4927 (2009).
33. K. Hiraoka, H. Finkelmann, *Macromol. Rapid Commun.* **22**, 456–460 (2001).
34. Z.-Q. Yu, J. W. Y. Lam, C.-Z. Zhu, E.-Q. Chen, B. Z. Tang, *Macromolecules* **46**, 588–596 (2013).
35. Y. Yao *et al.*, *Proc. Natl. Acad. Sci. U.S.A.* **115**, 12950–12955 (2018).
36. S. Li *et al.*, *Nature* **605**, 76–83 (2022).
37. S. Li, M. Aizenberg, M. M. Lerch, J. Aizenberg, *Acc. Mater. Res.* **4**, 1008–1019 (2023).

38. S. Li *et al*., *Adv. Mater.* **33**, e2105024 (2021).
39. Y. Klein, E. Efrati, E. Sharon, *Science* **315**, 1116–1120 (2007).
40. J. Kim, J. A. Hanna, M. Byun, C. D. Santangelo, R. C. Hayward, *Science* **335**, 1201–1205 (2012).
41. E. Nishikawa, H. Finkelmann, *Macromol. Chem. Phys.* **200**, 312–322 (1999).
42. A. S. Gladman, E. A. Matsumoto, R. G. Nuzzo, L. Mahadevan, J. A. Lewis, *Nat. Mater.* **15**, 413–418 (2016).
43. P. M. L. Janssen, M. Periasamy, *J. Mol. Cell. Cardiol.* **43**, 523–531 (2007).
44. M. Stålfelt, *Physiol. Plant.* **15**, 772–779 (1962).
45. Y. Forterre, J. M. Skotheim, J. Dumais, L. Mahadevan, *Nature* **433**, 421–425 (2005).
46. M. D. Rueda-Contreras, A. F. Gallen, J. R. Romero-Arias, A. Hernandez-Machado, R. A. Barrio, *Sci. Rep.* **11**, 9562 (2021).
47. Z. Zhou, R. Mittal, *Bioinspir. Biomim.* **13**, 015001 (2017).
48. M. Lahikainen, H. Zeng, A. Priimagi, *Nat. Commun.* **9**, 4148 (2018).
49. Scripts for: Y. Yao *et al*., Programming liquid crystal elastomers for multistep ambidirectional deformability, Harvard Dataverse (2024); https://dataverse.harvard.edu/dataverse/ambidirectional.

ACKNOWLEDGMENTS

We thank M. Aizenberg for fruitful discussions. **Funding:** This work was supported by the US Department of Energy (DOE), Office of Science, Basic Energy Sciences (BES), under award number DE-SC0005247 (experiment and characterization) and the Harvard University Materials Research Science and Engineering Center (MRSEC) under award number DMR-2011754 (theory and computational studies). M.M.L. thanks The Netherlands Organization for Scientific Research (NWO VENI grant number VI.Veni.202.158). F.S. is supported by the Deutsche Forschungsgemeinschaft (DFG) in the form of a Walter Benjamin Fellowship (project number 520766332). This research used SMI 12-ID of the National Synchrotron Light Source II, a US DOE Office of Science User Facility operated for the DOE Office of Science by Brookhaven National Laboratory under contract number DE-SC0012704.
Author contributions: Conceptualization: Y.Y., A.M.W., M.M.L., X.W., J.A.; Funding acquisition: J.A., M.M.L., B.K., M.Z.; Investigation: Y.Y., A.M.W., B.L., M.M.L., X.W., M.Z., G.F., P.W., F.S., F.T., A.H.W.; Methodology: Y.Y., A.M.W., M.M.L., B.L., X.W., M.Z., G.F., P.W., F.T., A.H.W., S.L., R.B., T.C., B.K., J.A.; Project administration: J.A., B.K.; Supervision: J.A.; Visualization: Y.Y., A.M.W., B.L., F.S.; Writing – original draft: Y.Y., A.M.W., X.W., M.M.L., J.A.; Writing – review & editing: Y.Y., A.M.W., X.W., M.M.L., A.G., S.L., B.K., J.A. **Competing interests:** B.K. is also affiliated with Bosch Research, Watertown, MA, USA. The remaining authors declare no competing interests. **Data and materials availability:** All data supporting the findings of this study are available in the main text or the supplementary materials. Scripts for analyses can be found at Harvard Dataverse (*49*).

SUPPLEMENTARY MATERIALS

science.org/doi/10.1126/science.adq6434
Materials and Methods
Supplementary Text
Figs. S1 to S26
Table S1
References (*50*–*71*)
Movies S1 to S6

Submitted 23 May 2024; accepted 24 October 2024
10.1126/science.adq6434